How to cite: *Angew. Chem. Int. Ed.* **2024**, *63*, e202411472
doi.org/10.1002/anie.202411472

Protein NMR Spectroscopy

Allostery at a Protein-Protein Interface Harboring an Intermolecular Motional Network

*Sara Medina Gomez, Tye I. Gonzalez, Suresh K. Vasa, and Rasmus Linser**

Abstract: Motional properties of proteins govern recognition, catalysis, and regulation. The dynamics of tightly interacting residues can form *intra*molecular dynamic networks, dependencies fine-tuned by evolution to optimize a plethora of functional aspects. The constructive interaction of residues from *different* proteins to assemble *inter*molecular dynamic networks is a similarly likely case but has escaped thorough experimental assessment due to interfering association/dissociation dynamics. Here, we use fast-MAS solid-state ^{15}N $R_{1\rho}$ NMR relaxation dispersion aided by molecular-dynamics simulations to mechanistically assess the hierarchy of individual µs timescale motions arising from a crystal-crystal contact, in the absence of translational motion. In contrast to the monomer, where particular mutations entail isolated perturbations, specific intermolecular interactions couple the motional properties between distant residues in the same protein. The mechanistic insights obtained from this conceptual work may improve our understanding on how intramolecular allostery can be tuned by intermolecular interactions via assembly of dynamic networks from previously isolated elements.

Adding to structure and site-specific chemical properties, motion constitutes a main pillar of protein functionality. In addition to translational motion and association/dissociation events, internal dynamics enable rather substantial changes between distinct conformations of vastly differential properties. In addition, more subtle local fluctuations are equally important for the thermodynamic feasibility of such conformations, transitions, binding affinities, and chemical conversion.[1] Such dynamics are inherently dependent on a complex array of internal and external parameters. Hence, they allow the effective modulation of protein functionality as a function of upstream regulators, feedback loops, and other conditions.[2]

*Intra*molecular dynamic networks between residues with mutually dependent motional properties allow allosteric communication between spatially distant sites,[3] a regulatory tool fine-tuned by evolution to optimally orchestrate the various aspects of protein function.[4] Orthosteric interaction partners, like small-molecule active-site ligands, can simply block interaction sites locally. By contrast, dynamic networks allow information flux from allosteric access points far away to tune local functionality. This allows selectivity despite, e.g., conservation of active sites across enzyme families.[1,5] This impact can be derived from global shifts in conformational ensembles, e.g., stabilization of individual conformations out of a more heterogeneous energy landscape, upon inhibitor binding to sites spatially distant from the active site.[6] Hence, binding-(in)competent or catalytically (un)productive conformations can be enriched.[7] Whereas in some cases, discrete conformations can be captured, other cases are not associated with appreciable structural differences to the apo protein. Here, an impact specifically onto the required protein dynamics is assumed.[8]

The interactions formed upon association of two or more interacting proteins are thought to create new, intermolecular dynamic networks that are capable of transducing information between the individual proteins.[9] These motional dependencies, in particular regarding conformational exchange on the µs timescale, are hard to capture with any of today's structural-biology techniques. Therefore, their mechanistic assessment by combined simulation and experimental verification within the breadth of regulatory protein-protein complexes, including very different lifetimes, has remained very limited. For example, as opposed to a rigidifying effect of *small-molecule* binders,[10] including allosteric modulators,[6d,11] it is conceivable that the association of a *protein* binding partner can extend a network, introducing motional coupling of otherwise decoupled regions within a protein in a *constructive* way. Such modulation (formation) of dynamic networks could be effective in modulating intramolecular information flux, rather than just abrogating dynamics by an added steric demand. This would effectively alter thermodynamic properties (e.g., affinities) of the ensemble even for short lifetimes of the individual complexes formed within a dynamic equilibrium.

To test the (hypothetical) possibility of such protein-protein interactions recoupling formerly uncoupled sites, we elucidate motional dependencies between two adjacent sides in a pocket of an SH3 domain. This "pincer-like" structure,

[*] Dr. S. Medina Gomez, T. I. Gonzalez, Dr. S. K. Vasa, Prof. Dr. R. Linser
Department of Chemistry and Chemical Biology
TU Dortmund University
Otto-Hahn-Str. 4a, 44227 Dortmund, Germany
E-mail: rasmus.linser@tu-dortmund.de

in a biological context, plays the role of sandwiching their proline-rich peptide ligands in a broad range of regulatory cascades (see a visualization of the cavity in Figure S1) and has found much interest in past work.[12] Capturing the internal motional properties of interest would usually be compromised by interfering association/dissociation dynamics between protein and peptide. For that reason, the cavity is interrogated bound to residues of another SH3 monomer within a crystal-crystal contact that is known to mimic the biological binding of target peptides.[12b] On the basis of our previous research,[13] we anticipated this interface to harbor a µs timescale motional network. Introducing local perturbations and reading out the respective changes in the vicinity, we succeed in identifying a hierarchy of individual µs timescale backbone conformational-exchange dynamics that effectively couple two sites that do not bear a physical connection in the monomeric protein.

The *RT* loop in the monomeric SH3 domain of chicken α-spectrin in solution displays a rich spectrum of intrinsic flexibility.[13b,14] In previous work, we showed that in the context of a crystal lattice, some of its motional modes are slowed down to the µs regime, making it responsive to $R_{1\rho}$ NEar Rotary resonance Relaxation Dispersion (NERRD). These experiments in the framework of fast magic-angle spinning and proton detection provide a selective readout of motional features specifically on the 10 µs timescale.[15] Comparison of experimental with simulated data for two-site exchange with different potential excited-state conformations suggested a backbone flip for residue R21, at the very tip of the *RT* loop, as a statistically justified explanation.[13b] The cavity it forms together with the *n-Src* loop is well accessible in the apo monomer (Figure S1). Interestingly, in the case of a crystalline lattice, residue 21 of the *RT* loop forms intermolecular interactions with the C- and the N-terminus of a second monomer, which also contact the *n-Src* loop, in particular N38, of the first monomer. Figure 1A shows the embedding of the central residue R21 at the protein-protein interface. Curious about the possible interplay of motional events in this particular sandwich architecture, we created specific local perturbations by mutating residue R21 while leaving everything else identical. (See the Supporting Information for preparative details.) In the monomeric protein in solution, a mutation to alanine can be confirmed to show the expected behavior of a *local* perturbation and incurs major chemical-shift perturbations (CSPs) only at the very mutation site (Figure 1B, C and F). The same is true for the replacement of R21 with aspartate, affording very similar CSPs as R21A. (See the SI, Figure S2, for solution HSQCs and CSPs of the R21E mutant.) In the framework of the crystal (with the same lattice as the wt, see Figure S3[13b,14]), by much contrast, the R21A mutation entails CSPs in *several* areas of the protein primary sequence (Figure 1D, E and F). Naively, these changes could simply be due to altered electrostatic effects sensed by *multiple* proximal residues at the monomer-monomer interface, even though they would be surprisingly widespread.

To interrogate the system in more detail, we looked closely at protein *dynamics* and their changes upon mutation. At first, we recorded a set of Redfield relaxation data for ^{15}N for wt protein and R21A mutant in solution (R_1, R_2, and heteronuclear steady-state NOE) and performed a reduced spectral-density mapping (Figures S4 and S5). Figure 2A compares the R_2 rates of wt and mutant as a measure that best represents contributions from both, fast and slow motions. Given the local character of the perturbation, no changes are introduced for the adjacent side of the binding cavity (residue N38). In the presence of the interactions within the crystal, by much contrast, motional properties are altered not only at the mutation site. Figure 2B shows that, on one hand, the $R_{1\rho}$ rate of position 21 at 20 kHz spin lock field strength slightly rises from around 10.7 to 12.7 s^{-1}. More interestingly, dynamics here seem to also be affected at the N- and C-terminus, the sidechain of W41, and, in particular, N38. $R_{1\rho}$ rates for these residues at 20 kHz spin lock field strength increase from 0.9 to 4.9, from 6.1 to 8.8, and from 5.6 to 12.0 s^{-1} for L61, W41ε, and N38, respectively (Figure 2B,C). Matching our observations, N38 dynamics in the wt crystal have previously been described to be surprisingly different from the solution state.[13a] D62 and E7

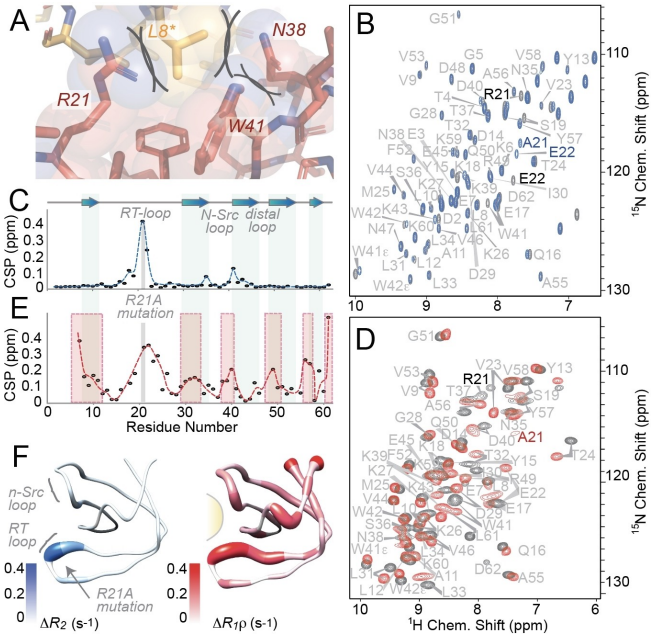

Figure 1. Steric context of the SH3 peptide binding pocket in the crystalline state and effects of its mutation. **A)** Zoom-in on the intermolecular interactions across the pocket in SH3 crystals, using PDB structure 2NUZ. R21 and N38, with a distance of ca. 12 Å, as well as intermittent residues touching each other, are annotated. Red and yellow structures denote a first and a second monomer, respectively. Heavy-atom van-der-Waals radii are depicted as semi-transparent. The asterisk for L8 denotes it belonging to the top monomer. **B)** Overlay of HSQCs for wt (gray) and mutant (blue) SH3 in solution. **C)** Chemical-shift perturbations of the R21A mutation in solution. **D)** Overlay of solid-state NMR H/N correlations for wt (gray) and mutant (red) SH3. **E)** Chemical-shift perturbations of the R21A mutation in the crystal. Regions affected on top of the local effect (gray line) are marked by red boxes. **F)** Depiction of CSPs in solution (left) and solids (right) on the SH3 structure. The yellow shape symbolizes the intermolecular interactions at the pocket.

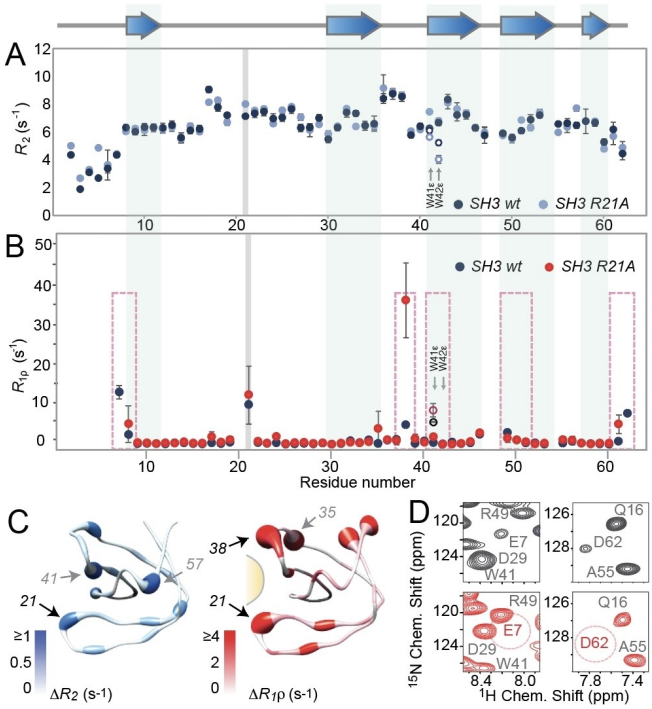

Figure 2. Local vs. global changes in the protein's motional properties. **A)** Solution NMR ^{15}N R_2 rates as a function of sequence. R21A data corrected by the minor global decrease in R_2 by ca. 0.5 s^{-1} (compare Figure S4) seen probably due to slightly decreased tumbling correlation times/Stokes radius. **B)** Solid-state NMR ^{15}N $R_{1\rho}$ rates at 20 kHz spin lock field strength. **C)** ^{15}N R_2 (left) and $R_{1\rho}$ data (right) from panels A) and B), respectively, plotted on the structure. **D)** Weakening of E7 and D62 signals in wt and mutant protein in hNH experiments.

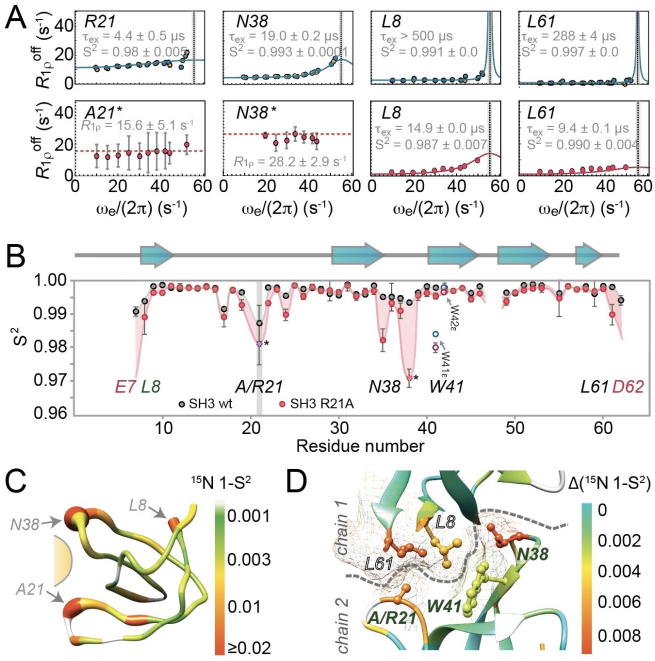

Figure 3. ^{15}N $R_{1\rho}$ NERRD data and localization of the motional impact of R21 mutation. **A)** NERRD profiles for residues 21, 38, 8, and 61 in the wt (top) and mutant protein (bottom). The flat line with a high y-axis offset obtained as the best fit for A21 and N38 in the mutant denotes motion exceeding the timescale window accessible for NERRD. **B)** NERRD-derived order parameters (referring to µs timescale conformational exchange only) as a function of sequence. For A21 and N38 in the case of the mutant (asterisks and dashed data points), NERRD fits were used even though their fast-motional behavior violates the χ^2-based significance criterion ($p < 0.05$) compared to a flat line. The trendline for the termini of the mutant is extrapolated to reflect that further reduced dipolar magnetization transfer efficiencies denote a further increase of motion. **C)** NERRD-derived 1-S^2 values for SH3 R21A depicted on the X-ray structure (2NUZ), representing µs mobility both, as ribbon thickness and via the color code shown, localized to the pocket and the N-terminus. **D)** Close-up of $\Delta(1\text{-}S^2)$ between wt and mutant, representing the red area in B), put into the context of the binding interface (between pocket and termini). X-ray structure of the R21A mutant: PDB 2F2W; the W41 value accords to the N_ε, which is more meaningful but almost identical to the backbone value, see B. The demarcation between monomers (chain 1, top, and chain 2, bottom) is depicted by a dashed line. Labels in bold (for A/R21, W41, and N38) denote residues belonging to the lower monomer, hollow font (L61 and L8) denotes resides belonging to the upper monomer. E7 and D62, now becoming highly mobile, are not shown. See Figure S11 for panels C and D plotted using a *one-color* gradient.

show very high $R_{1\rho}$ rates already in the wt (7.7 and 16.3 s^{-1}, respectively). These residues are not visible/fittable at all anymore in the mutant crystal due to a severely reduced signal-to-noise ratio. This signifies an even larger extent of motion in the mutant, now effectively evading the dipolar magnetization transfers even more than for the wt. Altogether, a flexibilization seems to happen exactly for those residues participating in the interface shown in Figure 1A.

In order to characterize the influence of the mutation onto the other spins in the neighborhood more specifically, we conducted ^{15}N NERRD measurements for wt and R21A mutant, for which a subset of data is shown in Figure 3A. ^{15}N NERRD exclusively assesses µs timescale H–N bond vector reorientation owing to partial recoupling of anisotropic interactions close to the rotor-resonance condition in $R_{1\rho}$ experiments at fast MAS.[15] For position 21, pronounced µs timescale dynamics are already observed in the wt protein.[13b,16] In the mutant, the expected further acceleration of its amide bond vector fluctuation, assumingly induced by the shortening and "discharging" of the R21 sidechain, becomes apparent. Upon decreasing the temperature of the measurement, the residue completely escapes quantitative characterization, presumably due to a combination of the low CP transfer efficiency with exchange broadening (Figure S6). In any case, a further increase in dynamics for A21 compared to R21 in the wild type is obvious. More importantly, in agreement with the above, we see the same mobilization also for residue N38, which equally transitions from a well-fittable profile into a situation similar to A21. L8 and L61 represent the most external residues of N- and C-terminus, respectively, that are still assessable in both constructs. These, as well as W41ε (compared in Figure S7), experience a notable onset of µs timescale motion. See a compilation of all NERRD profiles in Figs. S9 and S10. In addition, Figure S8 shows R_1 data, in which N38, L8, and W41ε are again increased, with N38 changing by more than a factor of two, i.e., from 0.07 to 0.18 s^{-1}. Figure 3B displays the fitted, NERRD-derived

order parameters of the individual residues as a function of sequence. Note that these only reflect the μs timescale contribution, which means values small in size compared to Redfield-type assessment of S^2 in solution. In addition to the NERRD-derived flexibility ($1\text{-}S^2$) for the wt protein before mutation, plotted on the structure in Figure 3C, Figure 3D shows the difference values between R21A and wt in the context of the interface. This increase of μs timescale backbone motion due to the mutation is also visualized in Figure 3B as a red shade.

An increase in flexibility in the surroundings of a mutation (in addition to flexibilization at the mutation site itself) could simply derive from the overall change (decrease) of steric restrictions. By contrast, dynamic networks are known to couple the motional properties of one with the *motional* characteristics of another residue. It is important to bear in mind that coupling on the atomic scale does not mean a simple transfer of impulse from one object to another as in coupled macroscopic systems. Instead, it denotes the conditional probabilities of stochastic, entropy-driven events, defined by their activation free energies, which depend on the surroundings, including conformational states temporarily adopted by vicinal residues.[17]

In order to capture the mechanistic underpinnings that would test the assumption of coupled dynamics for the chain of associated amino acids in the interface, we interrogated the interdependencies of conformational states via MD simulations. Even though, for the μs dynamics in focus, a sparse sampling of the events is expected, a qualitative view on the mechanism can thus be obtained. A simulation of the monomeric protein (bearing slightly reduced steric boundaries for R21 compared to the crystal) indeed returns the expected peptide flip reconstructed in previous NMR studies[13b] and from mixed crystallographic ground state structures for R21G mutation[14] (dark blue trace in Figure 4A). By contrast, the flip is not seen upon simulation of the protein within a crystalline lattice (see simulation details in the SI). This is again expected given the slow timescale of the process measured by solid-state NMR. (Figure S12 shows that one longer-lived flip is witnessed upon use of Gaussian-enhanced simulations.) R21 mutation to alanine, on the other hand, accelerates the flip in such a way that the simulation captures the event in total 16 times even in brute-force MD (Figure 3B), which enables further interrogation. No peculiar motion is discernable for N38 still (Figure S13), whose μs time motion is expected to be still too slow yet (fivefold slower NERRD profile than R21 in the wt protein). Additional simulations with a system prepared such that A21 starts in the *peptide-flipped* (excited) state—effectively increasing the time window for interrogating the consequences of the A21 excited state—are shown in Figure 4C. It is intriguing to see that, while (and only while) position 21 is in the peptide-flipped state, N38 in the same chain can undergo peptide flips itself (see Figure 4D, part of the trajectory for chain C): Four full transitions and two stretches with a partial rotation are seen during those 0.81 μs during which A21 is flipped. Else, for in total 3.29 μs over four chains, *no* backbone twist occurs, not even partially. (Also compare Figure S13.) The apparent dependency (the

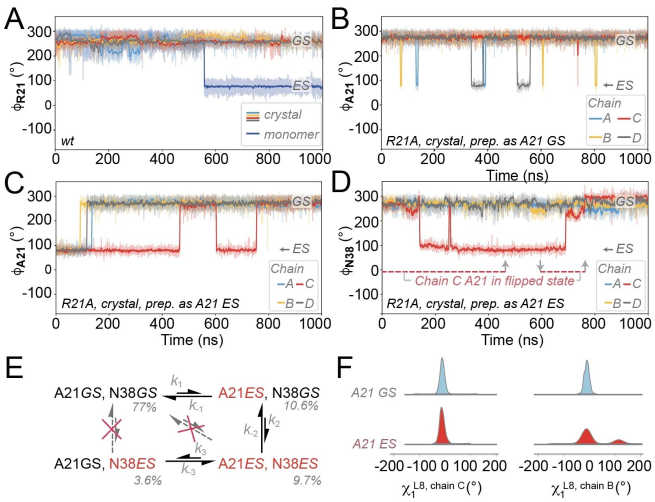

Figure 4. Elucidation of mechanistic dependencies by MD. **A)** R21 ϕ angle in the wt protein in monomeric (dark blue) and crystalline form (light blue, red, yellow, and gray, no observed flips) over 1 μs. **B)** Acceleration of the peptide flip in the crystal (using four individual monomers with contacts through periodic boundaries, see the Supporting Information for details) by R21A mutation. Monomers A, B, C, and D are represented by traces in blue, red, yellow, and gray, respectively. **C,D)** Simulation starting in A21 peptide-flipped state with C) A21 and D) N38 ϕ angle represented. **E)** Derived hierarchy of backbone conformational exchange, with transitions and relative residence times observed in the simulation over all four chains when starting with A21 flipped. Note that in the simulations, μs timescale events cannot be sampled sufficiently often to yield statistically sound quantification and the interpretations need to be kept at a qualitative level. **F)** L8 χ_1 angle distribution integrated over all frames bearing A21 in *GS* (blue) or those with A21 in *ES* (red).

modulation of transition probability for a second residue by the *state* of a first one) establishes a hierarchy of motional events, effectively coupling N38 backbone dynamics (their conditional probability) to the backbone dynamics of position 21. Even with a rather small periodic system, the simulation times accessible are insufficiently long for accurate sampling of μs timescale dynamics. Hence, flips violating this rule could still be expected to sporadically occur for longer sampling. But any *skewed* probability distribution, i.e., *less* N38 flips while A21 being in the excited state (*A21 ES*) than while in the ground state (*A21 GS*) would already suffice to conclude an impact onto downstream sites imposed by the state of the first residue. This conclusion seems a reasonable, qualitative interpretation within the technical limitations. To further interrogate this chain of events, we looked more closely at the mediating residue L8. In particular, we discriminated those MD frames harboring residue 21 in the *GS* from those with 21 in the *ES*. Whenever the system is in *A21 GS* state, the L8 sidechain χ_1 torsional angle is restricted to a single conformation. By contrast, in *A21 ES*, a bimodal distribution is obtained, in line with the relaxed steric boundaries for this situation (Figures 4F and S14). Interestingly, the individual L8 sidechain rotational states interchanging on a much faster timescale, this transmission again seems to act on the basis of *ensemble* properties (effective fast-timescale average of

L8 states) that depend on the state of the 21 backbone configuration. Unfortunately, *experimental* data for accurate determination of χ_1 flips under MAS is, as of now, hampered by technical hurdles.

The experiment also shows the *backbone* moieties of other residues to experience accelerated dynamics for the mutant, in particular L8, N61, and W41, now reaching the µs timescale. Unfortunately, specific motional mechanisms cannot be captured by MD as their backbone motions are too slow for the simulations. Also, what excited states they sample remains elusive. A similar specific dependency on the *state* (the dynamics, rather than average properties) of residue 21, as found for N38, is again possible. Alternatively, a simple decrease in spatial restrictions due to the mutation in general (irrespective of state) could equally apply.

The observed motional dependency suggests that intermolecular interactions are capable of tethering together spatial and motional (time-dependent spatial) properties of distant residues that, in the absence of the protein-protein interaction, are characterized by unrelated motion. In our case, these interactions are brought upon by the protein-protein interactions within a crystal lattice, providing mediating residues to "fill up" a vacancy of direct interactions between residues on adjacent sides of a binding pocket. The motional interdependencies are studied conceptually here, not for a specific biological case. Still, the witnessing of local motion as a feature dependent on the conformational states of a chain of neighboring residues being physically possible in this intermolecular sandwich arrangement implies a general mechanistic feasibility upon intermolecular association. We used methodology that specifically addresses µs timescale motion, in this case, the flipping of backbone dihedral angles, associated with comparably high activation barriers. However, the described kinetic dependencies should equally apply to other (faster or slower) timescales, amplitudes, and directionalities. In particular, we formulated the initial hypothesis that allosteric interaction partners might not only modulate information flux in dynamic networks destructively, e.g., through steric blockage or rigidification of protein segments. Instead, modulation might also happen in a constructive way, namely by adding missing connectivity between individual residues, inducing their hierarchical dynamic dependency by intermolecular association. This is indeed suggested by the various data gathered here, even though both, the experiments and simulations are limited by the mentioned boundaries. The assumption of such *constructive* mechanisms, altering the overall landscape of conformational entropy and motional interdependencies, might help to rationalize the aspect of dynamic allostery for modulated functionality or initiation of regulatory cascades and feedback loops induced by protein-protein interactions in future studies, as e.g., for binding/selectivity properties, enzymatic activity, and others, which has remained difficult to capture. Technically, gaining experimental access to long-range, intermolecular motional coupling across protein-protein interfaces without association/dissociation dynamics by solid-state NMR spectroscopy represents itself as an attractive approach to study biological conglomerates that are too short-lived for assessment of relaxation (dispersion) studies in solution.

In conclusion, using solid-state NMR and MD simulations to understand the perturbation of internal dynamics at a protein-protein interface induced by mutation, we gathered data that suggest that intermolecular dynamic networks can be formed upon protein-protein association by elements stemming from different partner proteins. The introduced interdependency between motions at otherwise uncoupled sections of the protein would create a means for information flux where no such connectivity exists in apo form. The physical principles deduced represent a generic possible mechanism for how dynamic allostery could be modulated in a constructive way by regulatory protein-protein interactions in biological signal transduction.

Chemical-shift assignments of the micro-crystalline R21A mutant in the solid state were deposited into the BMRB under accession code 52223.

Acknowledgements

We thank Dr. Petra Rovó (now IST Austria) for her committed help in setting this project up. Funded by the Deutsche Forschungsgemeinschaft (DFG, German Research Foundation) under Germany's Excellence Strategy—EXC 2033-390677874—RESOLV, and EXC-114-24286268—CiPS-M. Funded by the Deutsche Forschungsgemeinschaft (DFG, German Research Foundation)—27112786, 325871075 and the Emmy Noether program. Funded/Co-funded by the European Union (ERC, 101082494 bypassNMR). Views and opinions expressed are however those of the author(s) only and do not necessarily reflect those of the European Union or the European Research Council. Neither the European Union nor the granting authority can be held responsible for them. Open Access funding enabled and organized by Projekt DEAL.

Conflict of Interest

The authors declare no conflict of interest.

Data Availability Statement

The data that support the findings of this study are available in the supplementary material of this article.

Keywords: Solid-state NMR spectroscopy · Protein dynamics · Dynamic networks · Allostery

[1] H. van den Bedem, J. S. Fraser, *Nat. Methods* **2015**, *12*, 307–318.

[2] a) K. Gunasekaran, B. Ma, R. Nussinov, *Proteins Struct. Funct. Bioinf.* **2004**, *57*, 433–443; b) S. Bhattacharya, E. G. Margheritis, K. Takahashi, A. Kulesha, A. D'Souza, I. Kim, J. H. Yoon,

J. R. H. Tame, A. N. Volkov, O. V. Makhlynets, I. V. Korendovych, *Nature* **2022**, *610*, 389–393.
[3] a) J. Kuriyan, D. Eisenberg, *Nature* **2007**, *450*, 983–990; b) Kimberly, A. Reynolds, R. N. McLaughlin, R. Ranganathan, *Cell* **2011**, *147*, 1564–1575; c) H. Singh, C. K. Das, B. Buchmuller, L. V. Schäfer, D. Summerer, R. Linser, *Nucleic Acids Res.* **2023**, *51*, 6495–6506.
[4] a) H. G. Saavedra, J. O. Wrabl, J. A. Anderson, J. Li, V. J. Hilser, *Nature* **2018**, *558*, 324–328; b) A. Hadzipasic, C. Wilson, V. Nguyen, N. Kern, C. Kim, W. Pitsawong, J. Villali, Y. Zheng, D. Kern, *Science* **2020**, *367*, 912–917.
[5] a) S. R. Tzeng, C. G. Kalodimos, *Curr. Opin. Struct. Biol.* **2011**, *21*, 62–67; b) M. Vendruscolo, *Nat. Chem. Biol.* **2011**, *7*, 411–412.
[6] a) J. A. Hardy, J. A. Wells, *Curr. Opin. Struct. Biol.* **2004**, *14*, 706–715; b) J. W. Biddle, R. Martinez-Corral, F. Wong, J. Gunawardena, *eLife* **2021**, *10*, e65498; c) A.-M. Cao, R. B. Quast, F. Fatemi, P. Rondard, J.-P. Pin, E. Margeat, *Nat. Commun.* **2021**, *12*, 5426; d) A. A. Wylie, J. Schoepfer, W. Jahnke, S. W. Cowan-Jacob, A. Loo, P. Furet, A. L. Marzinzik, X. Pelle, J. Donovan, W. Zhu, S. Buonamici, A. Q. Hassan, F. Lombardo, V. Iyer, M. Palmer, G. Berellini, S. Dodd, S. Thohan, H. Bitter, S. Branford, D. M. Ross, T. P. Hughes, L. Petruzzelli, K. G. Vanasse, M. Warmuth, F. Hofmann, N. J. Keen, W. R. Sellers, *Nature* **2017**, *543*, 733–737.
[7] T. Xie, T. Saleh, P. Rossi, C. G. Kalodimos, *Science* **2020**, *370*, eabc2754.
[8] a) A. Cooper, D. T. F. Dryden, *Eur. Biophys. J.* **1984**, *11*, 103–109; b) L. G. Ahuja, S. S. Taylor, A. P. Kornev, *IUBMB Life* **2019**, *71*, 685–696.
[9] M. A. Maria-Solano, J. Iglesias-Fernańdez, S. Osuna, *J. Am. Chem. Soc.* **2019**, *141*, 13049–13056.
[10] a) H. Singh, C. K. Das, S. K. Vasa, K. Grohe, L. V. Schäfer, R. Linser, *Angew. Chem. Int. Ed.* **2020**, *59*, 22916–22921; b) H. Singh, S. K. Vasa, H. Jangra, P. Rovó, C. Päslack, C. K. Das, H. Zipse, L. V. Schäfer, R. Linser, *J. Am. Chem. Soc.* **2019**, *141*, 19276–19288.
[11] J. M. Ostrem, U. Peters, M. L. Sos, J. A. Wells, K. M. Shokat, *Nature* **2013**, *503*, 548–551.
[12] a) S. Feng, J. K. Chen, H. Yu, J. A. Simon, S. L. Schreiber, *Science* **1994**, *266*, 1241–1247; b) A. Cámara-Artigas, M. Andújar-Sánchez, E. Ortiz-Salmerón, C. Cuadri, S. Casares, *Acta Crystallogr. D Biol. Crystallogr.* **2009**, *65*, 1247–1252.
[13] a) V. Chevelkov, Y. Xue, R. Linser, N. Skrynnikov, B. Reif, *J. Am. Chem. Soc.* **2010**, *132*, 5015–5017; b) P. Rovó, C. A. Smith, D. Gauto, B. L. de Groot, P. Schanda, R. Linser, *J. Am. Chem. Soc.* **2019**, *141*, 858–869.
[14] S. Casares, O. López-Mayorga, M. C. Vega, A. Cámara-Artigas, F. Conejero-Lara, *Proteins Struct. Funct. Bioinf.* **2007**, *67*, 531–547.
[15] a) V. Kurauskas, S. A. Izmailov, O. N. Rogacheva, A. Hessel, I. Ayala, J. Woodhouse, A. Shilova, Y. Xue, T. Yuwen, N. Coquelle, J.-P. Colletier, N. R. Skrynnikov, P. Schanda, *Nat. Commun.* **2017**, *8*, 145; b) T. Zinkevich, V. Chevelkov, B. Reif, K. Saalwächter, A. Krushelnitsky, *J. Biomol. NMR* **2013**, *57*, 219–235; c) P. Schanda, M. Ernst, *Prog. Nucl. Magn. Reson. Spectrosc.* **2016**, *96*, 1–46.
[16] P. Rovó, R. Linser, *ChemPhysChem* **2018**, *19*, 34–39.
[17] H. Kamberaj, A. van der Vaart, *Biophys. J.* **2009**, *97*, 1747–1755.

Manuscript received: June 18, 2024
Accepted manuscript online: August 19, 2024
Version of record online: October 14, 2024